Biogeosciences, 15, 6033–6048, 2018
https://doi.org/10.5194/bg-15-6033-2018

Biogeosciences Open Access EGU

Organic matter characteristics in yedoma and thermokarst deposits on Baldwin Peninsula, west Alaska

Loeka L. Jongejans[1], **Jens Strauss**[1], **Josefine Lenz**[1,2], **Francien Peterse**[3], **Kai Mangelsdorf**[4], **Matthias Fuchs**[1,5], **and Guido Grosse**[1,5]

[1]Alfred Wegener Institute Helmholtz Centre for Polar and Marine Research, Permafrost Research Section, Potsdam, Germany
[2]University of Alaska Fairbanks, Institute of Northern Engineering, Fairbanks, AK, USA
[3]Utrecht University, Department of Earth Sciences, Utrecht, the Netherlands
[4]Helmholtz Centre Potsdam – German Research Centre for Geosciences, Potsdam, Germany
[5]University of Potsdam, Institute of Earth and Environmental Sciences, Potsdam, Germany

Correspondence: Loeka L. Jongejans (loeka.jongejans@awi.de)

Received: 28 March 2018 – Discussion started: 13 April 2018
Revised: 6 September 2018 – Accepted: 7 September 2018 – Published: 15 October 2018

Abstract. As Arctic warming continues and permafrost thaws, more soil and sedimentary organic matter (OM) will be decomposed in northern high latitudes. Still, uncertainties remain in the quality of the OM and the size of the organic carbon (OC) pools stored in different deposit types of permafrost landscapes. This study presents OM data from deep permafrost and lake deposits on the Baldwin Peninsula which is located in the southern portion of the continuous permafrost zone in west Alaska. Sediment samples from yedoma and drained thermokarst lake basin (DTLB) deposits as well as thermokarst lake sediments were analyzed for cryostratigraphical and biogeochemical parameters and their lipid biomarker composition to identify the below-ground OC pool size and OM quality of ice-rich permafrost on the Baldwin Peninsula. We provide the first detailed characterization of yedoma deposits on Baldwin Peninsula. We show that three-quarters of soil OC in the frozen deposits of the study region (total of 68 Mt) is stored in DTLB deposits (52 Mt) and one-quarter in the frozen yedoma deposits (16 Mt). The lake sediments contain a relatively small OC pool (4 Mt), but have the highest volumetric OC content (93 kg m^{-3}) compared to the DTLB (35 kg m^{-3}) and yedoma deposits (8 kg m^{-3}), largely due to differences in the ground ice content. The biomarker analysis indicates that the OM in both yedoma and DTLB deposits is mainly of terrestrial origin. Nevertheless, the relatively high carbon preference index of plant leaf waxes in combination with a lack of a degradation trend with depth in the yedoma deposits indicates that OM stored in yedoma is less degraded than that stored in DTLB deposits. This suggests that OM in yedoma has a higher potential for decomposition upon thaw, despite the relatively small size of this pool. These findings show that the use of lipid biomarker analysis is valuable in the assessment of the potential future greenhouse gas emissions from thawing permafrost, especially because this area, close to the discontinuous permafrost boundary, is projected to thaw substantially within the 21st century.

1 Introduction

The Arctic region is warming twice as fast as the global mean (Overland et al., 2017). Ice-rich permafrost soils are particularly vulnerable to climate warming and susceptible to large-scale thermokarst processes. Thermokarst is the subsidence of ground resulting from the thawing of ice-rich permafrost (Grosse et al., 2013; Günther et al., 2013). Thermokarst lake development often starts with the coalescence of polygonal ponds after the degradation of ice wedges (Grosse et al., 2013). This is followed by the formation of a body of unfrozen ground underneath the lake (i.e., talik), and subsequently both the lake and talik grow and deepen. Thermokarst lake development can cease by drainage through lateral outflows formed by thermal erosion of ice wedge networks, by tapping of lakes due to coastal erosion, by vertical outflow through open taliks in regions

with thin permafrost or by infilling with sediment or encroaching vegetation (Burn and Smith, 1990; Jones and Arp, 2015; Lenz et al., 2016c). After lake loss, the remaining basins largely become vegetated and eventually permafrost can reform (Jones et al., 2012). Due to the different stages of lake development, thermokarst landscapes are highly dynamic and form complex patterns of landscape units (Jones et al., 2012; Lenz et al., 2016a).

Late Pleistocene, ice-rich syngenetic permafrost, known as yedoma, is especially prone to rapid and deep thaw processes (Schirrmeister et al., 2013). These deposits cover large regions of Siberia and Alaska (Kanevskiy et al., 2011; Schirrmeister et al., 2013; Strauss et al., 2017) and can reach a thickness of up to 50 m (Sher, 1997; Shur et al., 2012). Yedoma contains large syngenetic ice wedges and can have a ground ice content of up to 80 vol %, thus yedoma deposits are highly vulnerable to thermokarst processes (Kanevskiy et al., 2016; Ulrich et al., 2014).

Permafrost landscapes store large quantities of organic carbon (OC; Hugelius et al., 2014; Strauss et al., 2013) as the generally low decomposition rates, due to low soil temperatures and poor drainage, inhibit decomposition of organic matter (OM; Davidson and Janssens, 2006). Permafrost thaw and talik formation, however, allow for microbial decomposition of the previously freeze-locked OM, resulting in increased greenhouse gas emissions (in particular carbon dioxide and methane) into the atmosphere and enhancing the initial warming (Koven et al., 2015; Schuur et al., 2015; Strauss et al., 2017). Rapid and large-scale permafrost degradation of ice-rich permafrost, such as yedoma deposits, may constitute a positive feedback to atmospheric warming.

Due to the freezing conditions during and after accumulation, the OM stored in yedoma deposits is highly decomposable (Knoblauch et al., 2013; Schädel et al., 2014a; Strauss et al., 2017). Yedoma deposits contain on average less OC than DTLB deposits (e.g., Strauss et al., 2013); however, higher respiration rates from yedoma deposits have been observed compared to DTLB deposits (Dutta et al., 2006; Lee et al., 2012; Zimov et al., 2006). Moreover, previous studies found that the state of OM decomposition is more dependent on OM properties, rather than on the age (Knoblauch et al., 2013; Stapel et al., 2016). It is therefore crucial to characterize the size of the OC pools and the quality of the OM in both undisturbed as well as disturbed ice-rich permafrost landscapes, so that the potential contribution to future greenhouse gas release following permafrost degradation can be better constrained for each of the different landscapes.

This study aims to characterize the belowground OM stored in thermokarst-affected areas by analyzing sediment samples from yedoma deposits, drained thermokarst lake basin deposits and thermokarst lake sediments. Two main questions are addressed: (1) how much OC is stored and (2) what is the quality of the OM? We want to identify the OC pool size and the vulnerability. The latter depends on the state of decomposition (i.e., vulnerability to future decomposition), expressed as quality, where a high quality refers to well preserved material. In our analysis, we focus on cryostratigraphical (bulk density, absolute ice content) and biogeochemical parameters (total organic carbon, total nitrogen, carbon–nitrogen ratio and stable carbon isotopes) to estimate the OC pool size of the yedoma, DTLB and thermokarst lake sediments. In addition, lipid plant and soil specific biomarkers (*n*-alkanes and brGDGTs, respectively) were used to determine the source and quality of the OM pool.

2 Material and methods

2.1 Study area

The study sites are located on the western coast of the Baldwin Peninsula, which is surrounded by the Kotzebue Sound in northwest Alaska (66°40′ N, 162°15′ W; Fig. 1). The Baldwin Peninsula is part of the former landmass Beringia that remained unglaciated during the Late Pleistocene (Hopkins, 1982). The peninsula is located in the southern portion of the continuous permafrost zone and therefore close to the discontinuous permafrost boundary (Jorgenson et al., 2008). According to geological maps, the peninsula is largely composed of a sequence of marine, fluvial and glaciogenic sediments, which are well exposed along coastal bluffs and in some regions covered by loess-like deposits (Hopkins et al., 1961; Huston et al., 1990; Pushkar et al., 1999). This study represents the first characterization of yedoma deposits on Baldwin Peninsula. A field campaign in summer 2016 revealed several yedoma exposures in active retrogressive thaw slumps on the western coast of the peninsula that consisted of fine-grained, ice-rich permafrost deposits penetrated by large syngenetic ice wedges. These yedoma exposures were located in upland remnants, a setting which is typical for yedoma hills found in northeast Siberia (Schirrmeister et al., 2013). A large portion of the peninsula has been affected by severe permafrost degradation and multiple thermokarst lake basin generations are visible in satellite imagery (Fig. 1). The present-day climate is sub-Arctic with an average annual precipitation of 280 mm and a mean annual air temperature of −5.2 °C (US Climate Data, 2017).

2.2 Field work

Sampling of yedoma and drained thermokarst lake basin (DTLB) exposures and thermokarst lake sediments was carried out on the western coast of the Baldwin Peninsula in August 2016 (Table 1). Photographs of the exposures and the lake core are shown in Supplement Sect. 2.1. The samples were named as follows: the geographical region (BAL for Baldwin Peninsula), the year of sampling (16 for 2016), the setting (B for bluff, UPL for upland), the site numbers (here: 2, 4) and the sampling of an aquatic environment was indicated (L for lake) (Table 1).

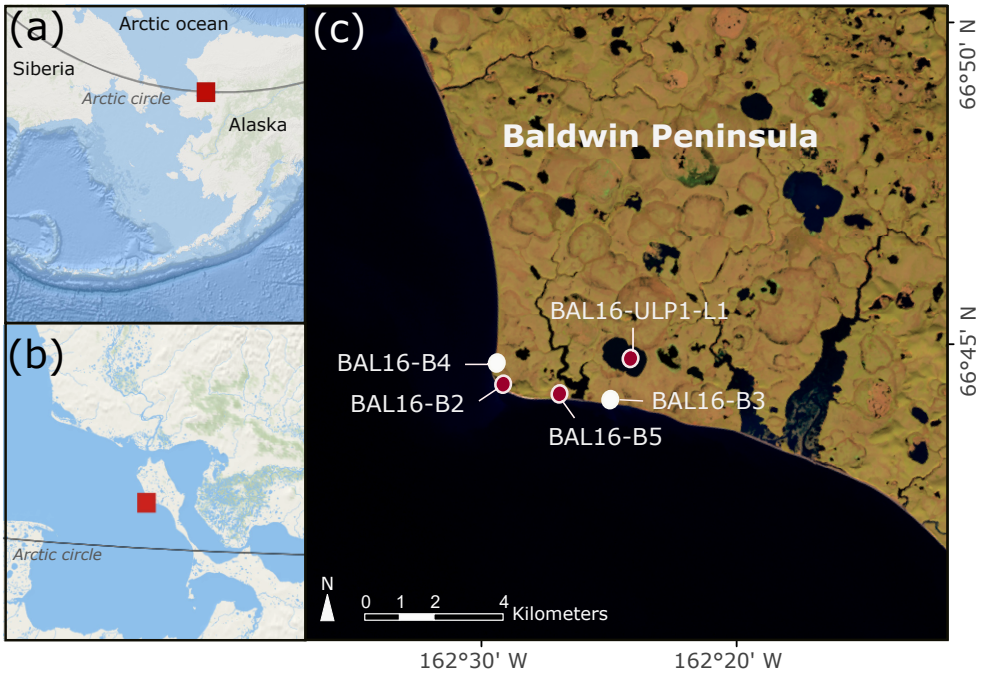

Figure 1. **(a)** Overview map of Siberia and Alaska with indicated study region (red square). **(b)** Close-up of Kotzebue Sound with indicated study region (red square). **(c)** Study sites on Baldwin Peninsula presented in this study (purple filled dots) and additional sites used in the organic carbon pool calculations (white dots); false color image with short-wave infrared, near-infrared and deep-blue bands (7-5-1); Source for background map in **(a)** and **(b)**: World Ocean Base (ESRI); satellite image map **(c)**: Landsat 8 image from 13 October 2016, USGS/NASA.

Table 1. Overview of study sites of yedoma exposure, drained thermokarst lake basin (DTLB) exposure and thermokarst lake sediments. BAL: Baldwin Peninsula, 16: expedition in 2016, B: bluff sampling, UPL: upland sampling, L: lake sampling.

Study site ID	Landscape unit	Coordinates	Samples, *n*
BAL16-B2	Yedoma exposure	66.73262° N, 62.49450° W	18
BAL16-B4	DTLB exposure	66.73644° N, 62.50208° W	31
BAL16-UPL1-L1	Thermokarst lake sediments	66.74220° N, 62.41310° W	9

A yedoma coastal bluff (BAL16-B2) of 16 m thickness was sampled. This bluff is characterized by sediments containing large ice wedges, ice bands and ice lenses, which are overlying a separate unit of ice-rich silty sediments. Due to the difficult terrain and fast thawing of the deposits in summer, it was not possible to sample the whole exposure in one straight profile. Therefore, 25 samples of the yedoma deposits were collected using a handheld power drill (ø 57 mm) at five different sampling locations along the exposure, forming a composite profile. Three additional samples were taken from the separate depositional unit underlying the yedoma, which was not as ice rich and did not contain in situ formed ice wedges. Exposures of DTLB deposits, ranging in thickness from 3 to 8 m, were sampled from three exposed profiles (BAL16-B3, BAL16-B4 and BAL16-B5). Thirty one samples were collected from the 8 m-high DTLB exposure BAL16-B4 consisting of mostly laminated sediments that contained various cryotextural and organic features (e.g., ice inclusions, lenses, organic matter inclusions). The DTLB exposures BAL16-B3 (9 samples) and BAL16-B5 (4 samples) were sampled to generate a broader sample base for the estimates of the DTLB OC pool (the results of the two DTLB additional profiles BAL16-B3 and BAL16-B5 are shown by depth in Supplement Sect. 2.3). All samples from the yedoma and DTLB exposures were kept frozen until laboratory analysis at the Alfred Wegener Institute (AWI), Helmholtz Centre for Polar and Marine Research, in Potsdam.

In addition, a 34 cm-long sediment core (BAL16-UPL1-L1) was retrieved from a shallow thermokarst lake (1.35 m deep at coring site) with a N–W extent, a length of about 1400 m and a width of 800 m. Unfrozen, slightly layered, clayey silty lake sediments were retrieved in a PVC tube (ø 60 mm) using a piston corer and were kept cool until subsampling (9 samples) and laboratory analysis.

2.3 Bulk physical properties

In the laboratory, the sediment samples were freeze-dried. The absolute ice content was derived from the weight difference of the frozen and dry samples after Eq. (1) and is expressed in weight percentage (wt %).

$$\text{Absolute ice content}\,(\text{wt}\,\%) = \frac{\text{wet weight–dry weight}}{\text{wet weight}} \cdot 100 \quad (1)$$

For the frozen samples, the bulk density BD_1 was calculated following Eq. (2).

$$BD_1\left(10^3\,\text{kg}\,\text{m}^{-3}\right) = (\varphi - 1)\cdot -\rho_s, \quad (2)$$

where φ is porosity (fraction) and ρ_s is the mineral density in (10^3 kg m^{-3}). The porosity is derived from the volumetric ratio of ice and dry sample whereby a constant ice density was assumed of 0.91×10^3 kg m^{-3} (at 0 °C; Lide, 1999). For the mineral density, the density of quartz of 2.65×10^3 kg m^{-3} was taken (Rowell, 1994).

For the unfrozen thermokarst lake sediments, BD_2 was calculated following Eq. (3). The volume of the sediment was corrected to account for the compression of the sediment during sampling. The volume of the excess water in the core tube after sampling was measured and included in the volume calculation of the core sediment.

$$BD_2\left(10^3\,\text{kg}\,\text{m}^{-3}\right) = \frac{\text{dry weight}}{\text{volume}}, \quad (3)$$

where dry weight is given in (g) and volume in (cm^3), respectively in (10^3 kg) and (m^3).

2.4 Radiocarbon dating

Macrofossils of 15 samples were dated by accelerator mass spectrometry (AMS) radiocarbon dating in the Radiocarbon Laboratory in Poznań, Poland (Goslar et al., 2004). The radiocarbon ages were calibrated using the CALIB 7.1 software and the IntCal13 calibration curve (Stuiver et al., 2017). All calibrated ages are expressed as calibrated kilo years before present (cal ka BP), including the standard deviation (±). Infinite ages (> 50 000 a) cannot be calibrated, and hence no uncertainty could be given.

2.5 Nitrogen and carbon content and composition

Homogenized samples were analyzed for total nitrogen (TN), total carbon (TC) and total organic carbon (TOC) using an elemental analyzer (Elementar Vario EL III and Elementar Vario Max C) and are expressed in (wt %). The TOC/TN weight ratio was calculated and will be referred to as C/N. The stable carbon isotopic composition was determined by measuring δ^{13}C (Thermo Fisher Scientific Delta-V-Advantage gas mass spectrometer equipped with a FLASH elemental analyzer EA 2000 and a CONFLO IV gas mixing system). The ratio is compared to the standardized Vienna Pee Dee Belemnite (VPDB) and expressed in per mille (‰ vs. VPDB). For samples with a TOC below the analytical accuracy (0.1 wt %), no C/N nor δ^{13}C was measured.

The combination of C/N and δ^{13}C has been widely used as an indicator of OM source. A higher C/N suggests an enhanced input of terrestrial land plants, whereas algal produced matter is generally characterized by a lower C/N. The C/N and δ^{13}C furthermore allow us to distinguish between marine and lacustrine algae, where marine algae generally have a higher δ^{13}C (e.g., Lenz et al., 2016a; Meyers, 1994, 1997). Moreover, the C/N and δ^{13}C have been used as an indicator of OM decomposition, where a lower C/N and higher δ^{13}C indicate further degraded material (i.e., lower quality; Gentsch et al., 2015; Gundelwein et al., 2007; Schädel et al., 2014b; Weiss et al., 2016a).

In order to compare the cryostratigraphy and biogeochemistry (BD, TOC, C/N and δ^{13}C) of the three stratigraphical landscape units (yedoma, DTLB and thermokarst lake deposits), the nonparametric Kruskal–Wallis test and Mann–Whitney–Wilcoxon test were performed using the R statistical environment to test for significant differences. When the p value exceeds 0.05, the null hypothesis (H_0: there is no statistically significant difference between the sample means of the different stratigraphic landscape units) cannot be rejected. In these statistical tests, the landscape units are treated separately, and therefore the internal differences in the study sites with depth and age are not included.

More extensive method descriptions of the elemental analysis can be found in Supplement Sect. 1.2.

2.6 Lipid biomarker analysis

2.6.1 Extraction and separation

Biomarker analysis was carried out to identify the OM composition and quality (Andersson and Meyers, 2012; Strauss et al., 2015). In total, 13 samples (6 from BAL16-B2 and 7 from BAL16-B4) were analyzed at the German Research Centre for Geosciences (GFZ) for n-alkanes (long-chained, single-bonded hydrocarbons) and branched glycerol diakyl glycerol tetraethers (brGDGTs; bacterial membrane lipids). The methods were adapted from Schulte et al. (2000) and Strauss et al. (2015). About 8 g of each sample was extracted (Dionex 200 ASE extractor) using dichloromethane / methanol (DCM/MeOH, 99 : 1 v/v, heating phase 5 min, static phase 20 min at 75 °C and 106 Pa). Excess solvent was evaporated under N_2. A known amount of four internal standards was added: 5α-androstane, ethylpyrene, 5α-androstan-17-on and erucic acid. The samples were passed over a sodium sulfate column with n-hexane prior to separation by medium-pressure liquid chromatography (MPLC; Radke et al., 1980) into three fractions: aliphatic hydrocarbons, aromatic hydrocarbons and nitrogen-, sulfur-, and oxygen-containing (NSO) compounds. The dissolved extracts were injected into the MPLC system where they were led through a column and pre-

columns (thermally deactivated silica 100, 63–200 and 200–500 µm on top with ratio $\sim 7:1$) with *n*-hexane. The NSO-fraction was further manually separated into a polar and acid fraction using a KOH-impregnated silica gel column with DCM.

2.6.2 Measurements

The *n*-alkanes were measured as part of the aliphatic fraction using gas chromatography–mass spectrometry (GC-MS; Trace GC Ultra and MS DSQ, Thermo Electron Corporation) using helium as a carrier gas. The samples were vaporized (50 to 300 °C with 10 °C s^{-1}, 10 min isothermal holding) and led through a capillary column (BPX5; 22 mm × 50 m, film thickness 0.25 µm; Peters et al., 2005). The oven was programmed from 50 to 310 °C (3 °C min^{-1} and 30 min isothermal holding). The GC was linked to the MS to enable compound identification (ionization mode at 70 eV, 230 °C). Full scan mass spectra were obtained from m/z 50 to 600 Da (2.5 scans s^{-1}). Using the software XCalibur, the peaks in the GC-MS total ion current chromatogram were manually integrated. The *n*-alkanes were quantified by comparing the peak area of the target compounds to the applied internal standards.

The brGDGTs were measured as part of the acid fraction using high-performance liquid chromatography (Shimadzu LC-10AD HPCL device coupled to a Finnigan TS 7000 mass spectrometer with APCI interface). The compounds were separated at 30 °C over a Prevail Cyano column (2.1 × 150 mm, 3 µm; Alltech) preceded by a precolumn filter of the same material, which does not separate 5- and 6-methyl isomers. Each fraction was eluted isocratically with *n*-hexane (A) and isopropanol (B; 5 min. 99 % A and 1 % B, linear gradient to 1.8 % B within 40 min, in 1 min to 10 % B holding for 5 min and back to initial conditions in 1 min, held for 16 min) with a flow rate of 0.2 mL min^{-1}. The APCI device has a corona current of 5 µA, voltage of 5 kV; the vaporizer temperature is 350 °C and the capillary temperature 200 °C. The source operates with nitrogen sheath gas at 60 psi (414 kPa) without auxiliary gas. Full mass spectra were obtained at a scan rate of 0.33 s. The integration was performed in XCalibur and the quantification was performed by comparing the compound peaks to an Archaeol run.

2.6.3 Biomarker-derived indices

The carbon preference index (CPI) of the *n*-alkanes was calculated after Marzi et al. (1993) following Eq. (4), and the average chain length (ACL) after Poynter and Eglinton (1990) following Eq. (5).

$$\mathrm{CPI}_{23-33} = \frac{\sum_{i=n}^{m} C_{2i+1} + \sum_{i=n+1}^{m+1} C_{2i+1}}{2 \cdot \left(\sum_{i=n+1}^{m+1} C_{2i}\right)}, \quad (4)$$

where n is the starting dominating chain length divided by 2, m the ending dominating chain length divided by 2 and i the carbon number index.

$$\mathrm{ACL}_{23-33} = \frac{\sum i C_i}{\sum C_i}, \quad (5)$$

where i is the carbon number and C the concentration. For the calculation of both CPI and ACL, the interval of C_{23} to C_{33} was used. The ACL indicates the OM source, where higher land plants (i.e., vascular plants) are dominated by long-chain *n*-alkanes of 25 to 30 carbon atoms, whereas bacteria and algae contain mainly shorter chains of 15 to 20 carbon atoms (Killops and Killops, 2013; Strauss et al., 2015). The CPI is the odd-to-even predominance of the hydrocarbons and indicates the degree of degradation of the OM, where a lower value indicates further degraded material (Andersson and Meyers, 2012; Glombitza et al., 2009).

2.7 Landscape organic carbon pool estimation

A map of key landscape units (yedoma hills, DTLBs and thermokarst lakes) of the northern part of Baldwin Peninsula was developed in order to calculate the coverage for each landscape unit and to allow a first-order estimate of the belowground OC storage. Using a Landsat 8 satellite image (false color image with short-wave infrared, near-infrared and deep-blue bands, bands 7-5-1, pixel resolution 30 m) as well as a digital terrain model (DTM; grid cell resolution 5 m), the three main landscape units were manually mapped and digitized for the northern part of the Baldwin Peninsula ($\sim 450\,km^2$). A similar approach of operator-driven thermokarst mapping by manually digitizing landforms from remote-sensing imagery in combination with a DTM was successfully applied by Morgenstern et al. (2011) and Farquharson et al. (2016).

The TOC pool on Baldwin Peninsula was then estimated based on the deposit thickness, the spatial coverage, wedge ice volume (WIV), BD and TOC from the sampled exposures and cores (BAL16-B2 to B5 and BAL16-UPL1-L1) following Eq. (6).

$$\text{TOC pool (Mt)} = \frac{\text{thickness} \cdot \text{coverage} \cdot \frac{100-\text{WIV}}{\text{WIV}} \cdot \text{BD} \cdot \frac{\text{TOC}}{100}}{10^6}, \quad (6)$$

where the deposit thickness is given in (m), spatial coverage in (m^2), WIV in (vol %), BD in ($10^3\,kg\,m^{-3}$) and TOC in (wt %). The deposit thickness is based on a few field observations and for this first-order assessment it is assumed to be constant over the whole peninsula. Deeper deposits below frozen yedoma and DTLB are excluded due to unknown spatial coverage and thickness. Also, the deposits below lake sediments, potentially unfrozen in a talik, are not included in the calculation. The spatial coverage per landscape unit was calculated from the land coverage classification map. Strauss et al. (2013) calculated the average WIV for yedoma and DTLB deposits based on polygon size and ice-wedge width and depth. WIV was assumed to be zero for the thermokarst lake sediments. In order to compensate for

possibly non-continuous field sampling, weighted BD · TOC values over depth were used by value replication depending on depth interval. The data were extrapolated to the northern part of the Baldwin Peninsula (i.e., the mapped part). The volumetric OC pool was estimated according to Eq. (7).

$$\text{Vol. OC pool}\left(\mathrm{kg\,m^{-3}}\right) = \left(\frac{100-\mathrm{WIV}}{\mathrm{WIV}}\cdot \mathrm{BD}\cdot\frac{\mathrm{TOC}}{100}\right)\cdot 10^3 \quad (7)$$

The calculation for each landscape unit was performed separately using bootstrapping techniques, which included 10^4 iterations of random sampling with replacement, after which the mean and standard deviation were calculated. Because BD and TOC are correlated, paired values were used during the random sampling.

3 Results

3.1 Biogeochemical and biomarker proxies

3.1.1 Yedoma exposure

Radiocarbon dates for yedoma exposure BAL16-B2 range from > 50 000 to 10 000 cal a BP (Table 2). There is no consistent age–depth relationship: while a few samples, including the near-surface sample, have an infinite age, the second youngest sample is found at a depth of 1600 cm. The cryostratigraphical and biogeochemical parameters are presented by depth (Fig. 2). Depths are measured from the cliff top downwards for the yedoma and DTLB exposures, and from the sediment surface downwards for the thermokarst lake sediments. The BD of the yedoma deposits (mean: 0.80×10^3 kg m^{-3}, SD: 0.18) shows most variation in the bottom part up to 1117 cm. The TOC ranges between 0.1 and 4.7 wt % (mean: 1.9 wt %, SD: 1.1). The C/N varies between 4.4 and 14.0 (mean: 10.1, SD: 2.9) and does not show a trend with depth. The δ^{13}C is in the range of −24.8 ‰ to −28.3 ‰ (mean: −25.9 ‰, SD: 0.9) and shows most variation up to 1080 cm. Exposure BAL16-B2 is very ice-rich with an average absolute ice content of 45 wt % (70 vol %).

The biomarker concentrations and index values are presented by depth in Fig. 3. The *n*-alkane concentration in the yedoma deposits ranges from 0.5 to 1.8 mg g^{-1} TOC (mean: 1.0 mg g^{-1} TOC, SD: 0.5). The ACL_{23-33} varies between 28.8 in the bottom sample and 28.2 in the top with a peak of 30.0 at 1117 cm (mean: 28.8, SD: 0.6). The samples are dominated by *n*-alkane chains with a high number of carbon atoms: the dominating chains are $n\text{-}C_{29}$ and $n\text{-}C_{31}$ (Fig. S7 in the Supplement). The CPI_{23-33} is in the range of 9.0 to 13.6 (mean: 11.6, SD: 2.0) and does not show a trend over depth. The sample at 1399 cm has the maximum brGDGT concentration of 1.3 µg g^{-1} TOC, whereas the other samples have relatively low concentrations (mean: 0.5 µg g^{-1} TOC, SD: 0.5).

3.1.2 DTLB exposure

Radiocarbon ages for DTLB exposure BAL16-B4 (Table 2) are in the range from > 50 000 cal a BP (788 to 434 cm) to 240 cal a BP (22 cm) and show no age inversions: the lower samples are of infinite age and the near-surface sediments are the youngest and show Holocene ages. The BD decreases upwards in the profile and ranges between 1.27 and 0.29×10^3 kg m^{-3} (mean: 0.91×10^3 kg m^{-3}, SD: 0.3), a particularly strong decrease occurs from 280 to 215 cm (Fig. 2). The TOC (mean: 6.6 wt %, SD: 9.4) is higher in the interval from 250 to 22 cm than in the lower part, and strongly increases in the top 8 cm. The C/N increases towards the top, ranging from 11.3 at the bottom to 29.0 at the top (mean: 14.9, SD: 4.2). The δ^{13}C displays an opposite trend with higher values in the lower part (−25.8 ‰) and a decrease near the surface (−28.7 ‰) (mean: −27.2 ‰, SD: 0.7), and a sudden decrease at 280 to 250 cm. The exposure has an average absolute ice content of 41 wt % (67 vol %).

The *n*-alkane concentration reaches its maximum of 16.0 mg g^{-1} TOC in the bottom sample, whereas the other samples have much lower concentrations (mean: 4.3 mg g^{-1} TOC, SD: 5.4; Fig. 3). The ACL_{23-33} is higher than 28 for all samples except at 583 and 430 cm (mean: 28.3, SD: 0.4). The dominating *n*-alkane chains are $n\text{-}C_{27}$ and $n\text{-}C_{31}$ (Fig. S7). The CPI_{23-33} increases towards the top from 5.7 to 12.6 (mean: 8.8, SD: 2.1). The brGDGT concentration varies between 0 and 3.8 µg g^{-1} TOC with the peak at 160 cm below the surface (mean: 1.5 µg g^{-1} TOC, SD: 1.4).

3.1.3 Thermokarst lake sediments

The radiocarbon age of the thermokarst lake core BAL16-UPL1-L1 (Table 2) is 2010 cal a BP at a depth of 26.5–27.5 cm and 480 cal a BP at 19–20 cm. The sedimentological and biogeochemical parameters (Fig. 2) have a low variability along the core profile with a mean for BD of 0.78×10^3 kg m^{-3} (SD: 0.01), TOC of 14.4 wt % (SD: 0.5), C/N of 22.5 (SD: 0.6) and δ^{13}C of −28.5 ‰ (SD: 0.2). The δ^{13}C shows a slight decrease towards the lake sediment surface.

3.1.4 Statistical significance

We found significant differences ($p < 0.05$) for all (pairwise) comparisons of the biogeochemical parameters between the yedoma, DTLB and thermokarst lake deposits on Baldwin Peninsula (Supplement Sect. 2.6). The DTLB deposits have the highest BD and the thermokarst lake sediments the lowest. The TOC and C/N are highest in the thermokarst lake sediments followed by the DTLB and then the yedoma deposits, whereas the δ^{13}C shows an opposite trend.

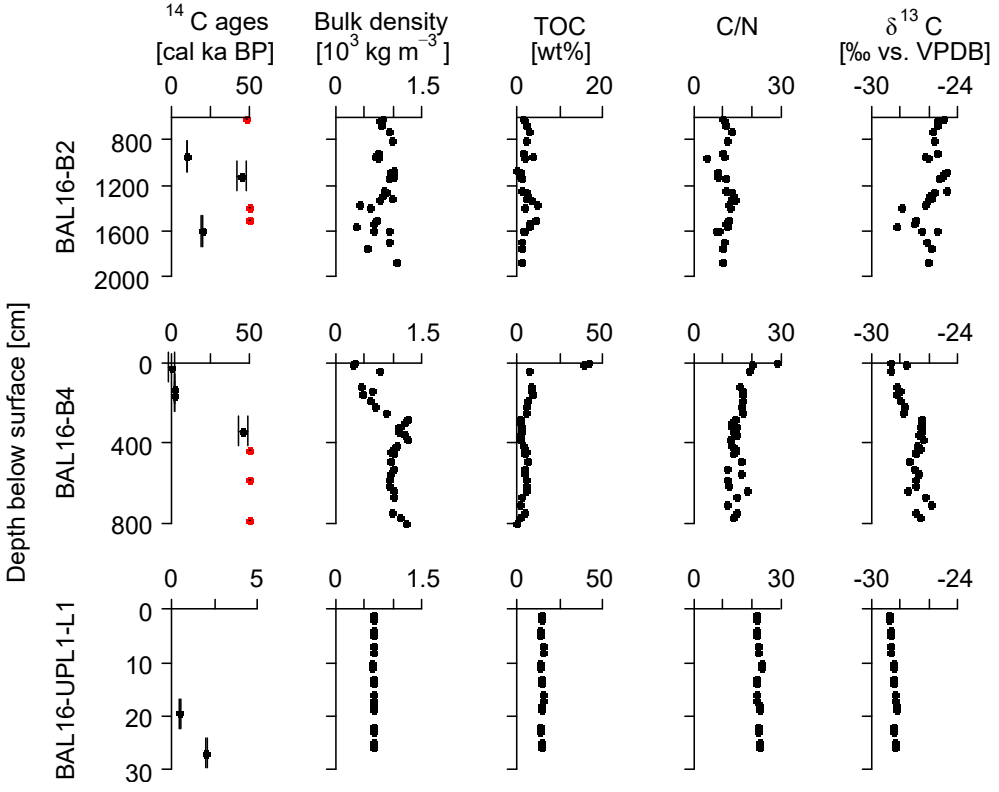

Figure 2. Summary of cryostratigraphical and biogeochemical parameters of BAL16-B2 (yedoma), BAL16-B4 (drained thermokarst lake basin) and BAL16-UPL1-L1 (thermokarst lake): calibrated radiocarbon ages (^{14}C; infinite ages in red), bulk density, total organic carbon (TOC), total organic carbon to total nitrogen ratio (C/N), stable carbon isotopes (δ^{13}C). Note: different x axes for ^{14}C and TOC.

Table 2. Radiocarbon dates of BAL16-B2 (yedoma), BAL16-B4 (drained thermokarst lake basin) and BAL16-UPL1-L1 (thermokarst lake). Calibrations were performed using CALIB 7.1 software and the IntCal13 calibration curve (Stuiver et al., 2017). Symbol ± for standard deviation; Poz: Poznań Radiocarbon Laboratory, Poland; pMC: percent modern carbon.

Sample ID	Ext. ID	Depth (cm)	^{14}C ages (a BP)	±	Calibrated ages 2σ (95.4 %) (a BP)	±	Rounded ^{14}C ages (cal a BP)	±
BAL16-B2-20	Poz-89527	620	> 48 000					
BAL16-B2-26	Poz-89700	945	8890	50	10 037.5	307	10 000	310
BAL16-B2-31	Poz-89702	1117	40 810	1800	44 747	6250	44 700	6250
BAL16-B2-39	Poz-89703	1399	> 50 000					
BAL16-B2-1	Poz-89526	1500	> 50 000					
BAL16-B2-5	Poz-89523	1600	16 200	90	19 551.5	575	19 600	580
BAL16-B4-2a	Poz-89704	22	105.7	0.33 pMC	239	30	240	30
BAL16-B4-4a	Poz-89705	132	1700	30	1590.5	93	1590	90
BAL16-B4-6a	Poz-89706	166	2125	30	2079.5	155	2080	160
BAL16-B4-14a	Poz-89707	340	42 800	1600	46 361.5	5935	46 400	6000
BAL16-B4-18a	Poz-89708	434	> 50 000					
BAL16-B4-24a	Poz-89709	583	> 50 000					
BAL16-B4-31a	Poz-89710	788	> 50 000					
BAL16-UPL1-L1-A	Poz-89349	19–20	425	30	482	86	480	90
BAL16-UPL1-L1-B	Poz-89351	26.5–27.5	1940	30	2014.5	129	2015	130

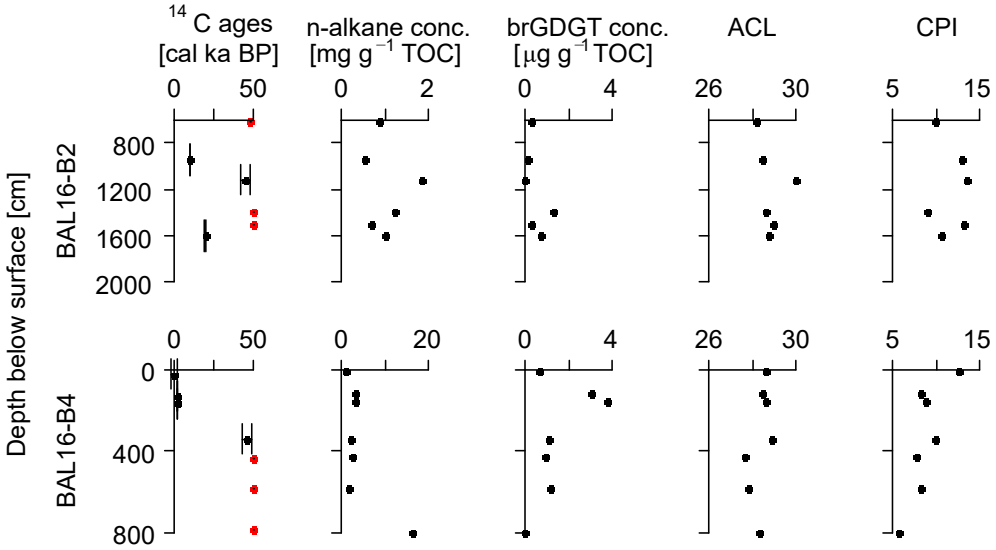

Figure 3. Summary of biomarker parameters of BAL16-B2 (yedoma) and BAL16-B4 (drained thermokarst lake basin): calibrated radiocarbon ages (^{14}C; infinite ages in red), *n*-alkane concentration, brGDGT concentration, average chain length (ACL) and carbon preference index (CPI). ACL and CPI were calculated from *n*-alkane range C_{23-33}. Note: radiocarbon ages are the same as in Fig. 2; different *x* axes for *n*-alkane concentration.

3.2 Organic carbon pool estimation

We produced a land cover classification map distinguishing between yedoma, DTLBs, thermokarst lakes and lagoons (Fig. 4). For the lakes on yedoma uplands and lagoons, no field information is available, so that those areas are excluded from further OC pool calculations. The total area mapped is about 450 km^2 of which ∼ 65 % is covered by DTLB, ∼ 30 % by yedoma and ∼ 5 % by thermokarst lakes (Table 3). The input parameters of the bootstrapping for the OC pool estimates are shown in Table 3. The volumetric and TOC pool per stratigraphic landscape unit for the frozen deposits and unfrozen thermokarst lake sediments are presented in Table 3, where the WIV is included. The OC pool estimates without WIV are also reported to allow for comparison with other studies (Table 3). The yedoma deposits contain 8.0 ± 0.8 kg OC m^{-3} (15.3 ± 1.6 excl. WIV) and the DTLB deposits 34.7±2.9 kg OC m^{-3} (37.4±3.1 excl. WIV), which corresponds to a TOC pool of 16.3±1.7 Mt (31.4±3.3 excl. WIV) in yedoma and 51.5 ± 4.3 Mt (55.4 ± 4.6 excl. WIV) in DTLB deposits. The total estimate of the TOC pool of the frozen sediments on northern Baldwin Peninsula is ∼ 68 Mt OC. The thermokarst lake sediments contain 92.9 ± 0.8 kg OC m^{-3}, which adds up to a TOC pool of 3.9 ± 0.0 Mt for all thermokarst lakes in the study area.

4 Discussion

4.1 Landscape development and carbon dynamics

4.1.1 Sediment facies

The yedoma deposits of BAL16-B2 have accumulated in a stable predominantly aeolian depositional environment, as shown by the grain size distribution (detailed method description and results of the grain size analysis are given in Supplement Sects. 1.1 and 2.5.1). The grain size distributions indicate that these deposits are characterized by a stronger aeolian influence than northeastern Siberian yedoma sites (Schirrmeister et al., 2008b; Strauss et al., 2012). Field observations suggest that the lower part of exposure BAL16-B2 (1600 to 1870 cm) is a separate unit. The significant change in sediment type from very coarse silt to medium silt (p value < 0.05), reflected in the grain size distributions (Supplement Sect. 2.5.1), confirms this distinction.

The formation of yedoma deposits on the west coast of the Baldwin Peninsula at study site BAL16-B2 possibly started before 50 cal ka BP. The wide range of radiocarbon ages in these yedoma deposits suggests that they are mixed with ancient or younger organic material. According to Vasil'chuk and Vasil'chuk (2017), contamination with ancient organic material is common in yedoma deposits, due to the syngenetic character of the deposits. Therefore, they proposed to take the youngest age of the sediments, justified by the fact that age rejuvenation is not likely, due to the undisturbed character of the deposits. However, it is unlikely that relatively young sediments (∼ 17 cal ka BP at 1600 cm) are overlain by a few meters of older sediments (∼ 45 cal ka BP

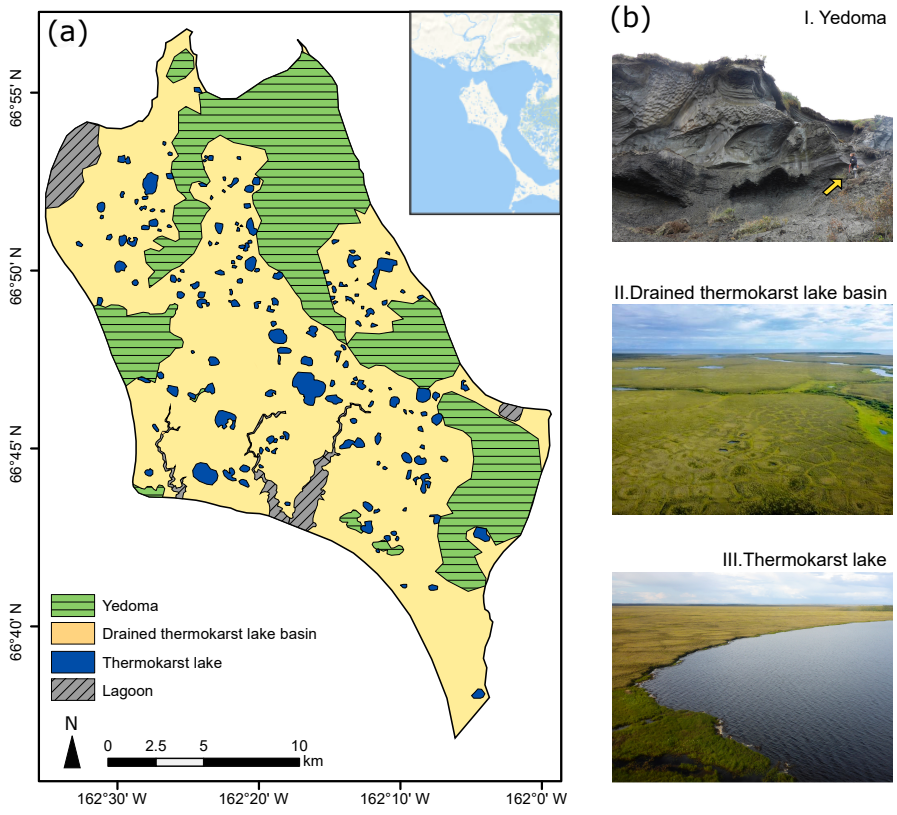

Figure 4. **(a)** Land cover classification map of Baldwin Peninsula (see overview map in upper-right corner) with yedoma (green), drained thermokarst lake basins (yellow), thermokarst lakes (blue) and lagoons (grey). **(b)** Exemplary photos: I. Yedoma (note person on the right indicated by yellow arrow for scale), II. Drained thermokarst lake basin and III. Thermokarst lake. Source for overview map in **(a)** is the World Ocean Base (ESRI).

Table 3. Input (left) and output parameters (right) for organic carbon pool calculations for yedoma, drained thermokarst lake basin and thermokarst lake deposits: deposit thickness, landscape coverage, wedge-ice volume (WIV). WIV data from Ulrich et al. (2014). Volumetric OC and TOC pools including and excluding WIV.

Landscape unit	Thickness (m)	Coverage (m^2)	WIV (vol %)	Volumetric OC pool Incl. WIV ($kg\,m^{-3}$)	TOC pool Incl. WIV (Mt)	Volumetric OC pool excl. WIV ($kg\,m^{-3}$)	TOC pool excl. WIV (Mt)
Yedoma	15	136 620 000	48	8.0 ± 0.8	16.3 ± 1.7	15.3 ± 1.6	31.4 ± 3.3
DTLB	5	296 440 000	7	34.7 ± 2.9	51.5 ± 4.3	37.4 ± 3.1	55.4 ± 4.6
Thermokarst lake	2	21 180 000	0			92.9 ± 0.8	3.9 ± 0.0

at 1117 cm and infinite ages at 1399 and 1500 cm), suggesting that the young ages could be the result of redeposition. Considering that BAL16-B2 is a coastal bluff, redeposition of young material cannot be neglected. Furthermore, the ages fall in the range of previous studies from Siberian yedoma deposits (> 57 to 13 ka BP; Schirrmeister et al., 2002a, b, 2003; Strauss et al., 2013) and Alaskan yedoma deposits (> 48 to 14 ka BP; Kanevskiy et al., 2011), except for the sample at 945 cm (∼ 10 cal ka BP). Generally, care should be taken with the interpretation of dating of yedoma deposits.

The lower part of the DTLB exposure BAL16-B4 has a radiocarbon age of 46 cal ka BP or older, which suggests that the lowest deposits have been accumulated during the same time as the yedoma formation. However, the TOC and C/N are significantly lower in BAL16-B2 than in BAL16-B4, whereas the $\delta^{13}C$ is significantly higher (Supplement Sect. 2.6). This suggests that the DTLB deposits are a mixture of former yedoma deposits thawed and partially decomposed in a lake talik, lake sediments and post-drainage terrestrial peat. The grain size signal for both exposures is

very similar ($p > 0.05$), suggesting a connection between the BAL16-B2 and BAL16-B4 sediments, which can be explained by the Holocene reworking of the yedoma sediments in the lake and in the talik affected by subsidence. The branched and isoprenoid tetraethers (BIT) index (detailed method description and results of the biomarker climatic indicator are given in Supplement Sects. 1.3 and 2.5.2) is lower for BAL16-B2 than for BAL16-B4, which may indicate that the sediments in BAL16-B2 have been deposited in a drier climate (Dirghangi et al., 2013), in line with earlier paleoenvironmental reconstructions (e.g., Andreev et al., 2011; Lenz et al., 2016c).

In exposure BAL16-B4 a change was observed in the proxy records (age, BD, TOC, δ^{13}C) between 280 and 250 cm: the sediments above 250 cm have lower BD and δ^{13}C and a higher TOC and C/N compared to the sediments below 280 cm. Furthermore, there is a change in sediment type, as shown by the different grain size distributions below 280 and above 250 cm (Supplement Sect. 2.5.1), and in the depositional environment, as shown by a change in the relative brGDGT distribution, reflected in the methylation of branched tetraethers (MBT) index (Supplement Sects. 1.3 and 2.5.2). These changes suggest the initiation of a thermokarst lake: the sediments below 280 cm are likely former yedoma sediments that were thawed in situ in a talik (taberite), whereas the upper sediments are lake sediments. The lake initiation likely happened during the Holocene. The drainage of the lake is not recorded in the data; the drainage event took place after 2.08 cal ka BP.

The thermokarst lake sediments from BAL16-UPL1-L1 have been accumulated during the Holocene (2010 and 480 a BP). Assuming a recent age for the surface sediments, the calculated sedimentation rate between 2010 and 480 years BP was $\sim 6\,\mathrm{cm\,ka^{-1}}$ and the sedimentation rate for the last 480 years $\sim 50\,\mathrm{cm\,ka^{-1}}$. For comparison, Lenz et al. (2016b) found a mean sedimentation rate for Peatball Lake, Alaska, of $\sim 70\,\mathrm{cm\,ka^{-1}}$ for the last 1400 years. The BD, TOC, C/N and δ^{13}C of the sediment core BAL16-UPL1-L1 show minimal variation, suggesting a stable depositional environment. Therefore, a hiatus in the sediment is unlikely.

4.1.2 Organic carbon quantity

To estimate future release of greenhouse gases from permafrost soils, the thaw-vulnerable OC pool needs to be identified. The OC quantity is identified by analyzing the TOC and estimating the OC budget. The thermokarst lake sediments have the highest TOC of the three landscape units, which is likely due to the addition of OM from lake primary production, as well as the integration of OM from its catchment. The DTLB deposits cover a wide range of TOC values, which corroborates the findings from Sect. 4.1.1 that the deposits are a mixture of reworked and new material. The TOC content of the yedoma deposits is comparable to TOC values reported in previous yedoma studies from across Siberia and Alaska (Fig. S6; Schirrmeister et al., 2008a, b, 2011; Strauss et al., 2012, 2013, 2015). Although the mean TOC content of the yedoma deposits is relatively low compared to that of DTLB deposits and thermokarst lake sediments, the volume of the yedoma deposits is of importance for the OC pool size, due to the large spatial coverage and thickness of deposits.

The thermokarst lake sediments ($\sim 93\,\mathrm{kg\,m^{-3}}$) have the highest volumetric OC pool compared to the yedoma and DTLB deposits. The DLTB deposits ($\sim 35\,\mathrm{kg\,m^{-3}}$) contain 4 times as much OC by volume as yedoma deposits ($\sim 8\,\mathrm{kg\,m^{-3}}$) and more than 2 times as much (DTLB: $\sim 37\,\mathrm{kg\,m^{-3}}$, yedoma: ~ 15) when excluding WIV. Multiple studies have been carried out to estimate OC pool size of deep yedoma and DTLB deposits. Here, we compare the volumetric OC pool to that of other studies excluding WIV, to compare the OC content of the frozen sediment only. Zimov et al. (2006) found that yedoma deposits contain on average $18.5\,\mathrm{kg\,m^{-3}}$ which is comparable to the yedoma deposits of Baldwin Peninsula. Furthermore, the DTLB OC pool of Baldwin Peninsula is in the range of 35.5 to 86.2 kg soil OC $\mathrm{m^{-3}}$ that Mueller et al. (2015) estimated for DTLB deposits in the Alaskan North Slope region. Schirrmeister et al. (2011; northeast Siberia; DTLB: 53.5, yedoma: 21.1–33.2 $\mathrm{kg\,m^{-3}}$) and Strauss et al. (2013; total yedoma region, $\sim 1\,387\,000\,\mathrm{km^2}$; DTLB: ~ 33, yedoma: $\sim 19\,\mathrm{kg\,m^{-3}}$) both estimated the OC budget of deep permafrost deposits (25 m deep) and found that DTLB deposits contain 1.5 to 2 times as much OC as yedoma deposits. Shmelev et al. (2017) found a slightly higher volumetric OC budget for thermokarst deposits ($14.2\,\mathrm{kg\,m^{-3}}$) than for yedoma deposits ($12.6\,\mathrm{kg\,m^{-3}}$).

On the other hand, Webb et al. (2017) also estimated the OC pool of Siberian deep deposits (0–15 m) and found that the yedoma deposits contained more OC (7.9 to 21.6 $\mathrm{kg\,m^{-3}}$) than the DTLB deposits (6.9 to 14.5 $\mathrm{kg\,m^{-3}}$). Other studies in Siberia (Fuchs et al., 2018; Siewert et al., 2016) also found more OC stored in yedoma deposits than in DTLB deposits. However, the estimates of these studies were based on near-surface sediments (0–2 m).

Based on our landscape unit map, we scaled the TOC pool of the Baldwin Peninsula. About 70 % of the area of Baldwin Peninsula is affected by permafrost degradation (e.g., thermokarst processes or coastal erosion) and is therefore classified as thermokarst. Moreover, these thermokarst processes led to more than 10 m of ground subsidence on the Baldwin Peninsula, as suggested by relief differences between yedoma uplands and DTLB. The estimated OC pool of the frozen sediments (yedoma 0–15 m depth, DTLB 0–5 m depth) on Baldwin Peninsula is ~ 68 Mt, of which roughly three-quarters (~ 52 Mt) is stored in DTLB deposits and one-quarter (~ 16 Mt) in yedoma deposits. This high amount of OC stored in an area of approximately $450\,\mathrm{km^2}$ shows the important contribution of these deep thermokarst-affected yedoma deposits to pan-Arctic soil OC stock estimations.

4.2 Organic matter quality

Permafrost conditions limit decomposition of OM, thereby preserving the quality. The OM quality is identified by analyzing the OM composition of the sediments. The source of OM influences both the quantity as well as the quality of OM. The ACL_{23-33} for both the yedoma (> 28.2) and DTLB (> 27.7) deposits suggests that the OM is mainly derived from terrestrial higher plants. Additionally, in all samples the long- and odd-chains dominate, which is also typical of a terrestrial higher plant origin (Eglinton and Hamilton, 1967).

Figure 5 shows a scatter plot of the C/N and δ^{13}C for the three landscape units of this study and other studies from Alaska: yedoma deposits along the Itkillik River (Lapointe et al., 2017; Strauss et al., 2012), DTLB deposits from the northern Seward Peninsula (Lenz et al., 2016c) and thermokarst lake sediments from lakes in the Kobuk River Delta and central Seward Peninsula (Lenz et al., 2018). We found significant statistical differences ($p < 0.05$) in almost all tests attempting to differentiate between OM composition in yedoma, DTLB and thermokarst lake deposits of the Baldwin Peninsula and the other Alaskan studies based on the C/N and the δ^{13}C (Supplement Sect. 2.6). A trend exists from a low C/N and high δ^{13}C in yedoma deposits towards a high C/N and low δ^{13}C in the thermokarst lake sediments (Fig. 5). Intermediate C/N and δ^{13}C were found for DTLB deposits. The high δ^{13}C and low C/N for the yedoma exposure (BAL16-B2) is typical (Dutta et al., 2006; Sánchez-García et al., 2014; Vonk et al., 2013), since it is characteristic of stadial periods with decreased productivity and a dry climate (Schirrmeister et al., 2011, 2013). The C/N and δ^{13}C of the DTLB deposits show a wide range, which reflects the mixed character of the disturbed landscape: these deposits contain, on the one hand, reworked OM (e.g., from former yedoma deposits) and, on the other hand, fresh OM (e.g., from thermokarst lake production). Thermokarst lake sediments are generally characterized by a low δ^{13}C (Cohen, 2003; Meyers, 1994), which is also the case here (Fig. 5). The high C/N of the thermokarst lake sediments is likely an indication that the OM is of high quality due to the contribution of fresh OM (Schirrmeister et al., 2013; Strauss et al., 2015). Hence, the trends of the C/N and δ^{13}C (Fig. 5) between the landscape units can be mainly explained by the source of the OM.

Comparing the properties of the OM pools per landscape unit at Baldwin Peninsula with the Alaskan study sites in Fig. 5 shows that the yedoma from Baldwin Peninsula does not have a significantly different C/N or δ^{13}C than that at Itkillik River ($p > 0.05$; Supplement Sect. 2.6), which suggests that the OM in both yedoma deposits has a similar composition. The DTLB deposits of Baldwin Peninsula have a significantly higher C/N ($p < 0.01$) compared to northern Seward Peninsula, but a similar δ^{13}C ($p > 0.05$). The lower C/N at northern Seward Peninsula can be explained by the

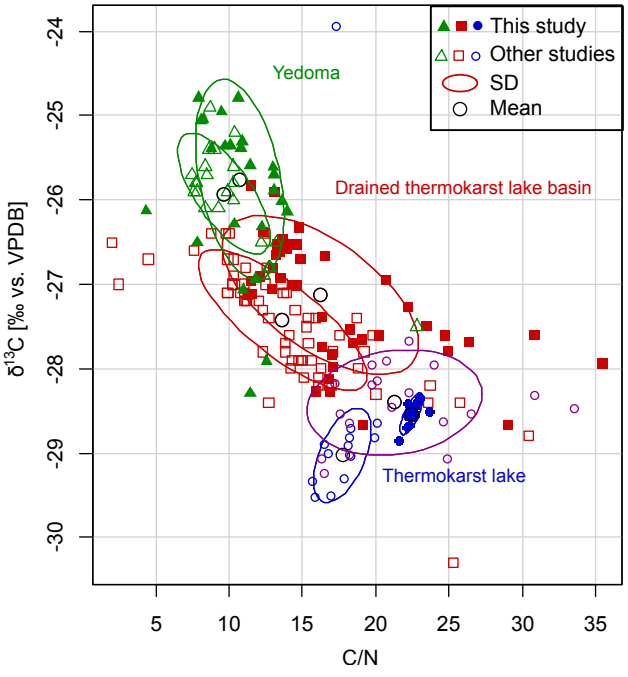

Figure 5. Scatter plot of total organic carbon to total nitrogen (C/N) ratio and stable carbon isotopes (δ^{13}C) of yedoma deposits (green triangles), drained thermokarst lake basin (DTLB) deposits (red squares) and thermokarst lake sediments (blue and purple dots) in Alaska. Mean values and standard deviations (SD) indicated. Data from this study (filled symbols): Baldwin Peninsula; data from other studies (hollow symbols): Itkillik River (Lapointe et al., 2017; Strauss et al., 2012), northern Seward Peninsula (Lenz et al., 2016a) and lakes from Kobuk River Delta (blue) and central Seward Peninsula (purple) (Lenz et al., 2018).

multiple lake generations this basin went through, leading to generally more degraded OM (Lenz et al., 2016a). Given that the C/N and δ^{13}C among thermokarst lakes at Baldwin Peninsula and central Seward Peninsula are significantly indistinguishable ($p > 0.05$), we argue that general contributions of lake production and thawed sediments from below are comparable, resulting in a similar OM composition. The thermokarst lake in the Kobuk River Delta, however, is significantly different in both proxies compared to the Baldwin Peninsula and central Seward Peninsula ($p < 0.01$). The lower δ^{13}C at the Kobuk River Delta can be an indication that the lacustrine contribution is higher than in Baldwin Peninsula and central Seward Peninsula. Nonetheless, the thermokarst lake sediments from Baldwin Peninsula, Kobuk River Delta and central Seward Peninsula all have a relatively high C/N and low δ^{13}C, compared to the yedoma and DTLB deposits (Fig. 5). The similar composition of the two yedoma study sites suggests a lack of decomposition, thereby implying the undisturbed character of the deposits. Furthermore, the differences in the DTLB study sites are likely caused by further OM composition in the northern Seward Peninsula

basin, which could have occurred during multiple lake generations the basin went through. These findings suggest that the range of the C/N and $\delta^{13}C$ within the study sites can be mainly explained by the quality of the OM.

A significantly higher CPI_{23-33} in yedoma compared to DTLB deposits (p value < 0.05) indicates that the OM in the yedoma deposits is less degraded and, therefore, suggests that this pool has a higher potential for future decomposition. Furthermore, the decreasing trend in CPI_{23-33} in the DTLB deposits indicates progressive degradation with depth, whereas the lack of such a trend in the yedoma deposits indicates that minimal or no decomposition has occurred before or after the OM was incorporated into the permafrost, maintaining its high quality (Stapel et al., 2016; Strauss et al., 2015; Weiss et al., 2016). These findings suggest that the OM in yedoma deposits BAL16-B2 is of higher quality than that in the DTLB deposits (BAL16-B4). Previous studies reported relatively high carbon turnover rates of Alaskan yedoma deposits (Dutta et al., 2006; Lee et al., 2012; Zimov et al., 2006), which suggest the presence of easily degradable OM in these deposits, which corroborates our findings.

Schuur et al. (2009) showed that in thermokarst-affected permafrost soils, old OM is released more strongly. Also, it was shown that the formation of mineral–organic associations can be an important factor influencing bioavailability of OM in permafrost soils, because it can improve the stability of OM in soils (Gentsch et al., 2015; Gundelwein et al., 2007; Höfle et al., 2013). Vonk et al. (2010) also showed the presence of this altered mineral-bound OM component in Arctic river and marine sediments. However, it is not clear yet how large the share of mineral-associated OM in permafrost soils is and how it exactly influences the stability in high-latitude soils (Höfle et al., 2013; Mueller et al., 2015).

Regardless, to evaluate implications of permafrost degradation arising from future climate change, it is necessary to assess the vulnerability of the total OM pool. Climate change will increase the frequency and intensity of fires and floods that can lead to soil removal and disturbances of the ground thermal regime, which can result in rapid local permafrost degradation (Grosse et al., 2011). Because of the high ice content in the yedoma and DTLB deposits on Baldwin Peninsula (> 45 vol %, excluding WIV), the deposits are highly susceptible and vulnerable to deep permafrost thaw, which will have a great effect on the topography. Lindgren et al. (2016) found a net increase in total lake surface area by 3.9 % for the Baldwin Peninsula between 1972 and 2014. With the formation of new deep lakes, primary productivity is expected to increase on a large scale, which will possibly compensate for increased greenhouse emissions initially. However, following the positive permafrost feedback loop, more intensive permafrost degradation will likely lead to an increase in the number of lake drainage events in west Alaska (Lindgren et al., 2016). This could lead to rapid OM sequestration in new permafrost aggrading in DTLBs and evolving terrestrial peat, but will be followed by ultimate decomposition once this region, which is ∼ 80 km from the discontinuous permafrost boundary (Brown et al., 1997), is affected by widespread permafrost near-surface thaw between 2050 and 2100 (Lawrence and Slater, 2005; Walter Anthony et al., 2014). Although the largest share of OC in frozen deposits on Baldwin Peninsula is stored in DTLB deposits (∼ 75 %), we showed that the OM in yedoma deposits is better preserved, and therefore the OM in the yedoma is especially vulnerable to future microbial degradation and greenhouse gas release that will further enhance climate warming.

5 Conclusions

This study presents OM characteristics from ice-rich yedoma and DTLB deposits and thermokarst lake sediments on the Baldwin Peninsula, west Alaska. We provide the first approximation of the size of the OC pools in ice-rich permafrost and the OM quality. Using cryostratigraphical, biogeochemical and biomarker parameters, the OC pool size of the frozen deposits is ∼ 68 Mt for the 450 km^2 study area of the Baldwin Peninsula. Frozen DTLB deposits make up 75 % of the TOC pool. The biomarker distributions showed a mainly terrestrial origin of the OM in both the yedoma and DTLB deposits. The lake sediments had the highest volumetric OC content of ∼ 93 kg OC m^{-3} compared to yedoma (∼ 8 kg OC m^{-3}) and DTLB deposits (∼ 35 kg OC m^{-3}). Biogeochemical and biomarker parameters indicated that the OM in the yedoma deposits is best preserved and of higher quality than the OM stored in DTLB deposits and thermokarst lake sediments. Thus, yedoma deposits have higher potential for OM decomposition, even though they make up only 25 % of the OC pool. Ongoing climate change will lead to the formation of deep thaw features and disturbances in yedoma permafrost. The rapid decomposition of the highly decomposable OM may potentially lead to significant greenhouse gas emissions.

Data availability. The data presented in this study are available on PANGAEA at https://doi.org/10.1594/PANGAEA.892310 (Jongejans et al., 2018).

The Supplement related to this article is available online at: https://doi.org/10.5194/bg-15-6033-2018-supplement

Author contributions. The study was designed by LLJ, JS and JL. Fieldwork was performed by JS, JL, MF and GG. Laboratory analysis was carried out by LLJ and FP, and KM provided input for the biomarker analysis and interpretation. The publication was written by LLJ with feedback from all authors.

Competing interests. The authors declare that they have no conflict of interest.

Acknowledgements. This study was carried out within the ERC PETA-CARB project (#338335) and additional support by the Helmholtz Impulse and Networking Fund (#ERC-0013). Loeka L. Jongejans was financially supported through an Erasmus+ EU grant. Field work was carried out by the Alfred Wegener Institute, Helmholtz Centre for Polar and Marine Research and the US Geological Survey (USGS). We thank the Kotzebue Community, Ben Jones (USGS), Jim Kincaid (Northwestern Aviation), Jim Webster (Webster's Flying Service) and Ingmar Nitze (AWI) for help in the field, and Dyke Scheidemann (AWI), Anke Sobotta and Cornelia Karger (German Research Centre for Geosciences) for their analytical support in the lab. We thank the editor and the anonymous referees for their helpful feedback.

The article processing charges for this open-access publication were covered by a Research Centre of the Helmholtz Association.

Edited by: Andreas Richter
Reviewed by: two anonymous referees

References

Andersson, R. A. and Meyers, P. A.: Effect of climate change on delivery and degradation of lipid biomarkers in a Holocene peat sequence in the Eastern European Russian Arctic, Org. Geochem., 53(Supplement C), 63–72, https://doi.org/10.1016/j.orggeochem.2012.05.002, 2012.

Andreev, A. A., Schirrmeister, L., Tarasov, P. E., Ganopolski, A., Brovkin, V., Siegert, C., Wetterich, S., and Hubberten, H.-W.: Vegetation and climate history in the Laptev Sea region (Arctic Siberia) during Late Quaternary inferred from pollen records, Quat. Sci. Rev., 30, 2182–2199, https://doi.org/10.1016/j.quascirev.2010.12.026, 2011.

Brown, J., Ferrians Jr., O., Heginbottom, J., and Melnikov, E.: Circum-Arctic map of permafrost and ground-ice conditions, https://doi.org/10.3133/cp45, US Geological Survey Reston, Virginia, 1997.

Burn, C. R. and Smith, M. W.: Development of thermokarst lakes during the holocene at sites near Mayo, Yukon territory, Permafr. Periglac. Process., 1, 161–175, https://doi.org/10.1002/ppp.3430010207, 1990.

Cohen, A. S.: Paleolimnology?: the history and evolution of lake systems, Oxford Univ. Press, Oxford, 2003.

Davidson, E. A. and Janssens, I. A.: Temperature sensitivity of soil carbon decomposition and feedbacks to climate change, Nature, 440, 165–173, https://doi.org/10.1038/nature04514, 2006.

Dirghangi, S. S., Pagani, M., Hren, M. T., and Tipple, B. J.: Distribution of glycerol dialkyl glycerol tetraethers in soils from two environmental transects in the USA, Org. Geochem., 59, 49–60, https://doi.org/10.1016/j.orggeochem.2013.03.009, 2013.

Dutta, K., Schuur, E. A. G., Neff, J. C., and Zimov, S. A.: Potential carbon release from permafrost soils of Northeastern Siberia, Glob. Change Biol., 12, 2336–2351, https://doi.org/10.1111/j.1365-2486.2006.01259.x, 2006.

Eglinton, G. and Hamilton, R. J.: Leaf Epicuticular Waxes, Science, 156, 1322–1335, https://doi.org/10.1126/science.156.3780.1322, 1967.

Farquharson, L., Anthony, K. W., Bigelow, N., Edwards, M., and Grosse, G.: Facies analysis of yedoma thermokarst lakes on the northern Seward Peninsula, Alaska, Sediment. Geol., 340, 25–37, https://doi.org/10.1016/j.sedgeo.2016.01.002, 2016.

Fuchs, M., Grosse, G., Strauss, J., Günther, F., Grigoriev, M., Maximov, G. M., and Hugelius, G.: Carbon and nitrogen pools in thermokarst-affected permafrost landscapes in Arctic Siberia, Biogeosciences, 15, 953–971, https://doi.org/10.5194/bg-15-953-2018, 2018.

Gentsch, N., Mikutta, R., Shibistova, O., Wild, B., Schnecker, J., Richter, A., Urich, T., Gittel, A., Šantručková, H., Barta, J., and others: Properties and bioavailability of particulate and mineral-associated organic matter in Arctic permafrost soils, Lower Kolyma Region, Russia, Eur. J. Soil Sci., 66, 722–734, 2015.

Glombitza, C., Mangelsdorf, K., and Horsfield, B.: Maturation related changes in the distribution of ester bound fatty acids and alcohols in a coal series from the New Zealand Coal Band covering diagenetic to catagenetic coalification levels, Org. Geochem., 40, 1063–1073, https://doi.org/10.1016/j.orggeochem.2009.07.008, 2009.

Goslar, T., Czernik, J., and Goslar, E.: Low-energy 14C AMS in Poznań Radiocarbon Laboratory, Poland, Nucl. Instrum. Methods Phys. Res. Sect. B Beam Interact. Mater. At., 223–224, 5–11, https://doi.org/10.1016/j.nimb.2004.04.005, 2004.

Grosse, G., Romanovsky, V., Jorgenson, T., Anthony, K. W., Brown, J., and Overduin, P. P.: Vulnerability and Feedbacks of Permafrost to Climate Change, Eos Trans. Am. Geophys. Union, 92, 73–74, https://doi.org/10.1029/2011EO090001, 2011.

Grosse, G., Jones, B., and Arp, C.: 8.21 Thermokarst Lakes, Drainage, and Drained Basins, in: Treatise on Geomorphology, edited by: Shroder, J. F., Giardino, R., and Harbor, J., Glacial and Periglacial Geomorphology, Academic Press, San Diego, 325–353, https://doi.org/10.1016/B978-0-12-374739-6.00216-52013, 2013.

Gundelwein, A., Müller-Lupp, T., Sommerkorn, M., Haupt, E. T. K., Pfeiffer, E.-M., and Wiechmann, H.: Carbon in tundra soils in the Lake Labaz region of arctic Siberia, Eur. J. Soil Sci., 58, 1164–1174, https://doi.org/10.1111/j.1365-2389.2007.00908.x, 2007.

Günther, F., Overduin, P. P., Sandakov, A. V., Grosse, G., and Grigoriev, M. N.: Short- and long-term thermo-erosion of ice-rich permafrost coasts in the Laptev Sea region, Biogeosciences, 10, 4297–4318, https://doi.org/10.5194/bg-10-4297-2013, 2013.

Höfle, S., Rethemeyer, J., Mueller, C. W., and John, S.: Organic matter composition and stabilization in a polygonal tundra soil of the Lena Delta, Biogeosciences, 10, 3145–3158, https://doi.org/10.5194/bg-10-3145-2013, 2013.

Hopkins, D. M.: Aspects of the paleogeography of Beringia during the Late Pleistocene, in: Paleoecology of Beringia, edited by: Hopkins, D. M., Matthews, J. V., Schweger, C. E., and Young, S. B., 3–28, Academic Press, New York, 1982.

Hopkins, D. M., McCulloch, D. S., and Jandra, R. J.: Pleistocene stratigraphy and structure of Baldwin Peninsula, Kotzebue Sound, Geol. Soc. Am. Spec. Pap., 68, 150–151, 1961.

Hugelius, G., Strauss, J., Zubrzycki, S., Harden, J. W., Schuur, E. A. G., Ping, C.-L., Schirrmeister, L., Grosse, G., Michaelson, G. J., Koven, C. D., O'Donnell, J. A., Elberling, B., Mishra, U., Camill, P., Yu, Z., Palmtag, J., and Kuhry, P.: Estimated stocks of circumpolar permafrost carbon with quantified uncertainty ranges and identified data gaps, Biogeosciences, 11, 6573–6593, https://doi.org/10.5194/bg-11-6573-2014, 2014.

Huston, M. M., Brigham-Grette, J., and Hopkins, D. M.: Paleogeographic significance of middle Pleistocene glaciomarine deposits on Baldwin Peninsula, northwest Alaska, Ann. Glaciol., 14, 111–114, 1990.

Jones, B. M. and Arp, C. D.: Observing a Catastrophic Thermokarst Lake Drainage in Northern Alaska, Permafr. Periglac. Process., 26, 119–128, https://doi.org/10.1002/ppp.1842, 2015.

Jones, M. C., Grosse, G., Jones, B. M., and Walter Anthony, K.: Peat accumulation in drained thermokarst lake basins in continuous, ice-rich permafrost, northern Seward Peninsula, Alaska, J. Geophys. Res.-Biogeo., 117, G00M07, https://doi.org/10.1029/2011JG001766, 2012.

Jongejans, L. L., Strauss, J., Lenz, J., Peterse, F., Mangelsdorf, K., Fuchs, M., and Grosse, G.: Sedimentological, biogeochemical and geochronological data of yedoma and thermokarst deposits in West-Alaska, available at: https://doi.pangaea.de/10.1594/PANGAEA.892310, 2018.

Jorgenson, M., Yoshikawa, K., Kanevskiy, M., Shur, Y., Romanovsky, V., Marchenko, S., Grosse, G., Brown, J., and Jones, B.: Permafrost characteristics of Alaska, Proceedings of the Ninth International Conference on Permafrost, vol. 29, 121–122, University of Alaska, Fairbanks, 2008.

Kanevskiy, M., Shur, Y., Fortier, D., Jorgenson, M. T., and Stephani, E.: Cryostratigraphy of late Pleistocene syngenetic permafrost (yedoma) in northern Alaska, Itkillik River exposure, Quat. Res., 75, 584–596, https://doi.org/10.1016/j.yqres.2010.12.003, 2011.

Kanevskiy, M., Shur, Y., Strauss, J., Jorgenson, T., Fortier, D., Stephani, E., and Vasiliev, A.: Patterns and rates of riverbank erosion involving ice-rich permafrost (yedoma) in northern Alaska, Geomorphology, 253, 370–384, https://doi.org/10.1016/j.geomorph.2015.10.023, 2016.

Killops, S. D. and Killops, V. J.: Introduction to Organic Geochemistry, Wiley, Somerset, 2013.

Knoblauch, C., Beer, C., Sosnin, A., Wagner, D., and Pfeiffer, E.-M.: Predicting long-term carbon mineralization and trace gas production from thawing permafrost of Northeast Siberia, Glob. Change Biol., 19, 1160–1172, https://doi.org/10.1111/gcb.12116, 2013.

Koven, C. D., Schuur, E. A. G., Schädel, C., Bohn, T. J., Burke, E. J., Chen, G., Chen, X., Ciais, P., Grosse, G., Harden, J. W., Hayes, D. J., Hugelius, G., Jafarov, E. E., Krinner, G., Kuhry, P., Lawrence, D. M., MacDougall, A. H., Marchenko, S. S., McGuire, A. D., Natali, S. M., Nicolsky, D. J., Olefeldt, D., Peng, S., Romanovsky, V. E., Schaefer, K. M., Strauss, J., Treat, C. C., and Turetsky, M.: A simplified, data-constrained approach to estimate the permafrost carbon–climate feedback, Philos. Trans. R. Soc. Math. Phys. Eng. Sci., 373, 20140423, https://doi.org/10.1098/rsta.2014.0423, 2015.

Lapointe, L. E., Talbot, J., Fortier, D., Fréchette, B., Strauss, J., Kanevskiy, M., and Shur, Y.: Middle to late Wisconsinan climate and ecological changes in northern Alaska: Evidences from the Itkillik River Yedoma, Palaeogeogr. Palaeoclimatol. Palaeoecol., 485, 906–916, https://doi.org/10.1016/j.palaeo.2017.08.006, 2017.

Lawrence, D. M. and Slater, A. G.: A projection of severe near-surface permafrost degradation during the 21st century, Geophys. Res. Lett., 32, 1–5, https://doi.org/10.1029/2005GL025080, 2005.

Lee, H., Schuur, E. A. G., Inglett, K. S., Lavoie, M., and Chanton, J. P.: The rate of permafrost carbon release under aerobic and anaerobic conditions and its potential effects on climate, Glob. Change Biol., 18, 515–527, https://doi.org/10.1111/j.1365-2486.2011.02519.x, 2012.

Lenz, J., Wetterich, S., Jones, B. M., Meyer, H., Bobrov, A., and Grosse, G.: Evidence of multiple thermokarst lake generations from an 11 800-year-old permafrost core on the northern Seward Peninsula, Alaska, Boreas, 45, 584–603, https://doi.org/10.1111/bor.12186, 2016a.

Lenz, J., Jones, B. M., Wetterich, S., Tjallingii, R., Fritz, M., Arp, C. D., Rudaya, N., and Grosse, G.: Impacts of shore expansion and catchment characteristics on lacustrine thermokarst records in permafrost lowlands, Alaska Arctic Coastal Plain, Arktos, 2, 25, https://doi.org/10.1007/s41063-016-0025-0, 2016b.

Lenz, J., Grosse, G., Jones, B. M., Walter Anthony, K. M., Bobrov, A., Wulf, S., and Wetterich, S.: Mid-Wisconsin to Holocene Permafrost and Landscape Dynamics based on a Drained Lake Basin Core from the Northern Seward Peninsula, Northwest Alaska, Permafr. Periglac. Process., 27, 56–75, https://doi.org/10.1002/ppp.1848, 2016c.

Lenz, J., Jones, B. M., Fuchs, M., and Grosse, G.: C/N and d13C data from short sediment cores from 9 lakes in Western Alaska, available at: https://doi.pangaea.de/10.1594/PANGAEA.887848, 2018.

Lide, D. R.: CRC handbook of chemistry and physics?: a ready-reference book of chemical and physical data, CRC Press, Boca Raton, 1999.

Lindgren, P., Grosse, G., and Romanovsky, V.: Landsat-Based Lake Distribution and Changes in Western Alaska Permafrost Regions Between 1972 and 2014, in XI International Conference on Permafrost, Potsdam, Germany, https://doi.org/10.2312/GFZ.LIS.2016.001, 2016.

Marzi, R., Torkelson, B. E., and Olson, R. K.: A revised carbon preference index, Org. Geochem., 20, 1303–1306, https://doi.org/10.1016/0146-6380(93)90016-5, 1993.

Meyers, P. A.: Preservation of elemental and isotopic source identification of sedimentary organic matter, Chem. Geol., 114, 289–302, https://doi.org/10.1016/0009-2541(94)90059-0, 1994.

Meyers, P. A.: Organic geochemical proxies of paleoceanographic, paleolimnologic, and paleoclimatic processes, Org. Geochem., 27, 213–250, https://doi.org/10.1016/S0146-6380(97)00049-1, 1997.

Morgenstern, A., Grosse, G., Günther, F., Fedorova, I., and Schirrmeister, L.: Spatial analyses of thermokarst lakes and basins in Yedoma landscapes of the Lena Delta, The Cryosphere, 5, 849–867, https://doi.org/10.5194/tc-5-849-2011, 2011.

Mueller, C. W., Rethemeyer, J., Kao-Kniffin, J., Löppmann, S., Hinkel, K. M., and Bockheim, J.: Large amounts of labile organic carbon in permafrost soils of northern Alaska, Glob. Change Biol., 21, 2804–2817, 2015.

Overland, J., Hanna, E., Hanssen-Bauer, I., Kim, S.-J., Walsh, J., Wang, M., Bhatt, U. S., and Thoman, R. L.: Surface Air Tem-

perature, available at: http://www.arctic.noaa.gov/Report-Card/Report-Card-2017 (last access: 13 December 2017), 2017.

Peters, K. E., Walters, C. C., and Moldowan, J. M.: The biomarker guide, 1, Biomarkers and isotopes in the environment and human history, Cambridge University Press, Cambridge, 2005.

Poynter, J. and Eglinton, G.: 14. Molecular composition of three sediments from hole 717c: The Bengal fan, Proceedings of the Ocean Drilling Program: Scientific results, vol. 116, 155–161, College Station, TX, 1990.

Pushkar, V. S., Roof, S. R., Cherepanova, M. V., Hopkins, D. M., and Brigham-Grette, J.: Paleogeographic and paleoclimatic significance of diatoms from middle Pleistocene marine and glaciomarine deposits on Baldwin Peninsula, northwestern Alaska, Palaeogeogr. Palaeoclimatol. Palaeoecol., 152, 67–85, https://doi.org/10.1016/S0031-0182(99)00040-1, 1999.

Radke, M., Willsch, H., and Welte, D. H.: Preparative hydrocarbon group type determination by automated medium pressure liquid chromatography, Anal. Chem., 52, 406–411, 1980.

Rowell, D. L.: Soil Science: methods & applications., Longman Scientific & Technical, University of Michigan, Michigan, 1994.

Sánchez-García, L., Vonk, J. E., Charkin, A. N., Kosmach, D., Dudarev, O. V., Semiletov, I. P., and Gustafsson, Ö.: Characterisation of Three Regimes of Collapsing Arctic Ice Complex Deposits on the SE Laptev Sea Coast using Biomarkers and Dual Carbon Isotopes, Permafr. Periglac. Process., 25, 172–183, https://doi.org/10.1002/ppp.1815, 2014.

Schädel, C., Schuur, E. A. G., Bracho, R., Elberling, B., Knoblauch, C., Lee, H., Luo, Y., Shaver, G. R., and Turetsky, M. R.: Circumpolar assessment of permafrost C quality and its vulnerability over time using long-term incubation data, Glob. Change Biol., 20, 641–652, https://doi.org/10.1111/gcb.12417, 2014a.

Schädel, C., Schuur, E. A. G., Bracho, R., Elberling, B., Knoblauch, C., Lee, H., Luo, Y., Shaver, G. R., and Turetsky, M. R.: Circumpolar assessment of permafrost C quality and its vulnerability over time using long-term incubation data, Glob. Change Biol., 20, 641–652, https://doi.org/10.1111/gcb.12417, 2014b.

Schirrmeister, L., Siegert, C., Kunitzky, V. V., Grootes, P. M., and Erlenkeuser, H.: Late Quaternary ice-rich permafrost sequences as a paleoenvironmental archive for the Laptev Sea Region in northern Siberia, Int. J. Earth Sci., 91, 154–167, 2002a.

Schirrmeister, L., Siegert, C., Kuznetsova, T., Kuzmina, S., Andreev, A., Kienast, F., Meyer, H., and Bobrov, A.: Paleoenvironmental and paleoclimatic records from permafrost deposits in the Arctic region of Northern Siberia, Quat. Int., 89, 97–118, https://doi.org/10.1016/S1040-6182(01)00083-0, 2002b.

Schirrmeister, L., Grosse, G., Schwamborn, G., Andreev, A., Meyer, H., Kunitsky, V. V., Kuznetsova, T., Dorozhkina, M. V., Pavlova, E. Y., Bobrov, A., and Oezen, D.: Late Quaternary history of the accumulation plain north of the Chekanovsky Ridge (Lena Delta, Russia) – a multidisciplinary approach, Polar Geogr., 27, 277–319, 2003.

Schirrmeister, L., Grosse, G., Kunitsky, V., Magens, D., Meyer, H., Dereviagin, A., Kuznetsova, T., Andreev, A., Babiy, O., Kienast, F., Grigoriev, M., Overduin, P. P., and Preusser, F.: Periglacial landscape evolution and environmental changes of Arctic lowland areas for the last 60 000 years (western Laptev Sea coast, Cape Mamontov Klyk), Polar Res., 27, 249–272, https://doi.org/10.1111/j.1751-8369.2008.00067.x, 2008a.

Schirrmeister, L., Kunitsky, V. V., Grosse, G., Kuznetsova, T. V., Derevyagin, A. Y., Wetterich, S., and Siegert, C.: The Yedoma Suite of the Northeastern Siberian Shelf Region characteristics and concept of formation, Proceedings of the Ninth International Conference on Permafrost, Fairbanks, Alaska, 2008b.

Schirrmeister, L., Grosse, G., Wetterich, S., Overduin, P. P., Strauss, J., Schuur, E. A. G., and Hubberten, H.-W.: Fossil organic matter characteristics in permafrost deposits of the northeast Siberian Arctic, J. Geophys. Res.-Biogeo., 116, 1–16, https://doi.org/10.1029/2011JG001647, 2011.

Schirrmeister, L., Froese, D., Tumskoy, V., Grosse, G., and Wetterich, S.: Yedoma: Late Pleistocene ice-rich syngenetic permafrost of Beringia, edited by: Elias, S. A., Mock, C. J., and Murton, J., Elsevier, Amsterdam, 2013.

Schulte, S., Mangelsdorf, K., and Rullkötter, J.: Organic matter preservation on the Pakistan continental margin as revealed by biomarker geochemistry, Org. Geochem., 31, 1005–1022, https://doi.org/10.1016/S0146-6380(00)00108-X, 2000.

Schuur, E. A., Vogel, J. G., Crummer, K. G., Lee, H., Sickman, J. O., and Osterkamp, T.: The effect of permafrost thaw on old carbon release and net carbon exchange from tundra, Nature, 459, 556–559, https://doi.org/10.1038/nature08031, 2009.

Schuur, E. A. G., McGuire, A. D., Schädel, C., Grosse, G., Harden, J. W., Hayes, D. J., Hugelius, G., Koven, C. D., Kuhry, P., Lawrence, D. M., Natali, S. M., Olefeldt, D., Romanovsky, V. E., Schaefer, K., Turetsky, M. R., Treat, C. C., and Vonk, J. E.: Climate change and the permafrost carbon feedback, Nature, 520, 171–179, https://doi.org/10.1038/nature14338, 2015.

Sher, A. V.: Yedoma as a store of paleoenvironmental records in Beringia, in: Beringia Palaeoenvironmental Workshop, edited by: Elias, S. and Bringham-Grette, J., 92–94, ON, Canada, 1997.

Shmelev, D., Veremeeva, A., Kraev, G., Kholodov, A., Spencer, R. G. M., Walker, W. S., and Rivkina, E.: Estimation and Sensitivity of Carbon Storage in Permafrost of North-Eastern Yakutia, Permafr. Periglac. Process., 28, 379–390, https://doi.org/10.1002/ppp.1933, 2017.

Shur, Y., Kanevskiy, M., Jorgenson, T., Dillon, M., Stephani, E., Bray, M., and Fortier, D.: Permafrost degradation and thaw settlement under lakes in yedoma environment, Proceedings of the Tenth International Conference on Permafrost, vol. 1, 5–29, Salekhard, Russia, 2012.

Siewert, M. B., Hugelius, G., Heim, B., and Faucherre, S.: Landscape controls and vertical variability of soil organic carbon storage in permafrost-affected soils of the Lena River Delta, CATENA, 147, 725–741, https://doi.org/10.1016/j.catena.2016.07.048, 2016.

Stapel, J. G., Schirrmeister, L., Overduin, P. P., Wetterich, S., Strauss, J., Horsfield, B., and Mangelsdorf, K.: Microbial lipid signatures and substrate potential of organic matter in permafrost deposits: Implications for future greenhouse gas production, J. Geophys. Res.-Biogeo., 121, 2652–2666, https://doi.org/10.1002/2016JG003483, 2016.

Strauss, J., Schirrmeister, L., Wetterich, S., Borchers, A., and Davydov, S. P.: Grain-size properties and organic-carbon stock of Yedoma Ice Complex permafrost from the Kolyma lowland, northeastern Siberia, Glob. Biogeochem. Cycles, 26, GB3003, https://doi.org/10.1029/2011GB004104, 2012.

Strauss, J., Schirrmeister, L., Grosse, G., Wetterich, S., Ulrich, M., Herzschuh, U., and Hubberten, H.-W.: The

deep permafrost carbon pool of the Yedoma region in Siberia and Alaska, Geophys. Res. Lett., 40, 6165–6170, https://doi.org/10.1002/2013GL058088, 2013.

Strauss, J., Schirrmeister, L., Mangelsdorf, K., Eichhorn, L., Wetterich, S., and Herzschuh, U.: Organic-matter quality of deep permafrost carbon – a study from Arctic Siberia, Biogeosciences, 12, 2227–2245, https://doi.org/10.5194/bg-12-2227-2015, 2015.

Strauss, J., Schirrmeister, L., Grosse, G., Fortier, D., Hugelius, G., Knoblauch, C., Romanovsky, V., Schädel, C., Deimling, T. S. von, Schuur, E. A. G., Shmelev, D., Ulrich, M., and Veremeeva, A.: Deep Yedoma permafrost: A synthesis of depositional characteristics and carbon vulnerability, Earth-Sci. Rev., 172, 75–86, https://doi.org/10.1016/j.earscirev.2017.07.007, 2017.

Stuiver, M., Reimer, P. J., and Reimer, R. W.: CALIB 14C Calibration Program, available at: http://calib.org/calib/ (last access: 13 December 2017), 2017.

Ulrich, M., Grosse, G., Strauss, J., and Schirrmeister, L.: Quantifying Wedge-Ice Volumes in Yedoma and Thermokarst Basin Deposits, Permafr. Periglac. Process., 25, 151–161, https://doi.org/10.1002/ppp.1810, 2014.

US Climate Data: Climate Kotzebue – Alaska, available at: https://www.usclimatedata.com/climate/kotzebue/alaska/united-states/usak0135/2017/1 (last access: 10 May 2017), 2017.

Vasil'chuk, Y. K. and Vasil'chuk, A. C.: Validity of radiocarbon ages of Siberian yedoma, Geo. Res. J., 13(Supplement C), 83–95, https://doi.org/10.1016/j.grj.2017.02.004, 2017.

Vonk, J. E., Van Dongen, B. E., and Gustafsson, Ö.: Selective preservation of old organic carbon fluvially released from sub-Arctic soils, Geophys. Res. Lett., 37, L11605, https://doi.org/10.1029/2010GL042909, 2010.

Vonk, J. E., Mann, P. J., Davydov, S., Davydova, A., Spencer, R. G. M., Schade, J., Sobczak, W. V., Zimov, N., Zimov, S., Bulygina, E., Eglinton, T. I., and Holmes, R. M.: High biolability of ancient permafrost carbon upon thaw, Geophys. Res. Lett., 40, 2689–2693, https://doi.org/10.1002/grl.50348, 2013.

Walter Anthony, K. M., Zimov, S. A., Grosse, G., Jones, M. C., Anthony, P. M., III, F. S. C., Finlay, J. C., Mack, M. C., Davydov, S., Frenzel, P., and Frolking, S.: A shift of thermokarst lakes from carbon sources to sinks during the Holocene epoch, Nature, 511, 454–456, https://doi.org/10.1038/nature13560, 2014.

Webb, E. E., Heard, K., Natali, S. M., Bunn, A. G., Alexander, H. D., Berner, L. T., Kholodov, A., Loranty, M. M., Schade, J. D., Spektor, V., and Zimov, N.: Variability in above- and belowground carbon stocks in a Siberian larch watershed, Biogeosciences, 14, 4279–4294, https://doi.org/10.5194/bg-14-4279-2017, 2017.

Weiss, N., Blok, D., Elberling, B., Hugelius, G., Jørgensen, C. J., Siewert, M. B., and Kuhry, P.: Thermokarst dynamics and soil organic matter characteristics controlling initial carbon release from permafrost soils in the Siberian Yedoma region, Sediment. Geol., 340, 38–48, https://doi.org/10.1016/j.sedgeo.2015.12.004, 2016a.

Weiss, N., Blok, D., Elberling, B., Hugelius, G., Jørgensen, C. J., Siewert, M. B., and Kuhry, P.: Thermokarst dynamics and soil organic matter characteristics controlling initial carbon release from permafrost soils in the Siberian Yedoma region, Sediment. Geol., 340, 38–48, https://doi.org/10.1016/j.sedgeo.2015.12.004, 2016b.

Zimov, S. A., Davydov, S. P., Zimova, G. M., Davydova, A. I., Schuur, E. A. G., Dutta, K., and Chapin, F. S.: Permafrost carbon: Stock and decomposability of a globally significant carbon pool, Geophys. Res. Lett., 33, L20502, https://doi.org/10.1029/2006GL027484, 2006.